Observation of Collisionless Shocks in Laser-Plasma Experiments

L. Romagnani,[1,*] S. V. Bulanov,[2,3] M. Borghesi,[1] P. Audebert,[4] J. C. Gauthier,[5] K. Löwenbrück,[6] A. J. Mackinnon,[7] P. Patel,[7] G. Pretzler,[6] T. Toncian,[6] and O. Willi[6]

[1]*School of Mathematics and Physics, The Queen's University of Belfast, Belfast, Northern Ireland, United Kingdom*
[2]*APRC, JAEA, Kizugawa, Kyoto, 619-0215 Japan*
[3]*Prokhorov Institute of General Physics RAS, Moscow, 119991 Russia*
[4]*Laboratoire pour l'Utilisation des Lasers Intenses (LULI), UMR 7605 CNRS-CEA-École Polytechnique-Univ, Paris VI, 91128 Palaiseau, France*
[5]*Université Bordeaux 1; CNRS; CEA, Centre Lasers Intenses et Applications, 33405 Talence, France*
[6]*Institut für Laser–und Plasmaphysik, Heinrich-Heine-Universität, Düsseldorf, Germany*
[7]*Lawrence Livermore National Laboratory, Livermore, California 94550, USA*

(Received 4 April 2008; published 10 July 2008)

The propagation in a rarefied plasma ($n_e \lesssim 10^{15}$ cm^{-3}) of collisionless shock waves and ion-acoustic solitons, excited following the interaction of a long ($\tau_L \sim 470$ ps) and intense ($I \sim 10^{15}$ W cm^{-2}) laser pulse with solid targets, has been investigated via proton probing techniques. The shocks' structures and related electric field distributions were reconstructed with high spatial and temporal resolution. The experimental results were interpreted within the framework of the nonlinear wave description based on the Korteweg–de Vries–Burgers equation.

DOI: 10.1103/PhysRevLett.101.025004 PACS numbers: 52.35.Tc, 41.75.Jv, 52.35.Sb, 52.50.Jm

The study of collisionless shocks and their relation to ion-acoustic solitons has received a great deal of attention in the past both from the experimental and theoretical point of view as well as in connection with space-plasma physics observations. Solitons can be regarded as fundamental nonlinear entities, and their connections range from nonlinear wave dynamics in shallow water to the quantum field theory [1]. Collisionless shock waves play a fundamental role in a number of astrophysical processes [2]. Charged particle energization at the front of collisionless shock waves generated during supernova explosions is believed to provide the main acceleration mechanism for cosmic rays [3]. In the laser-plasma physics context the observation of collisionless shocks was reported by several authors [4], often aiming to reproduce astrophysical phenomena in small scale laboratories. However, in general when the shocks were observed with optical probing techniques the front structure could not be resolved, thus making it impossible to distinguish between different shock typologies.

In this Letter we present the experimental observation of the propagation of laser-excited collisionless shocks in a low density plasma ($n \lesssim 10^{15}$ cm^{-3}). The shocks are generated following the sudden expansion of a dense plasma into a rarefied ionized background [5]. The dense plasma is produced via direct laser ablation of a solid target with a relatively long ($\tau_L \sim 470$ ps) and intense ($I \sim 10^{15}$ W/cm^2) laser pulse. It is assumed that the ambient plasma, where the shocks are excited and propagate, is created via photoionization of the residual gas in the target chamber, mainly driven by the thermal radiation emitted from the laser-heated target [5]. The shocks are observed employing a laser-accelerated proton beam as a charged particle probe. The electric field distribution and the shocks' structures have been reconstructed with high spatial and temporal resolution. This permitted the identification of different shock typologies, which were identified as the typical stationary solutions of the Korteweg–de Vries–Burgers (KdV-B) equation (and of its dissipationless limit, i.e., the Korteweg–de Vries (KdV) equation), namely, collisionless shock waves (KdV-B) and ion-acoustic solitons (KdV).

The experiment was carried out employing the LULI 100 TW laser system operating in the chirped pulse amplification mode (CPA). After stretching and amplification the main CPA pulse was split into two separate CPA_1 and CPA_2 pulses. CPA_1 was employed in the chirped uncompressed mode, providing a 470 ps long laser pulse which was focused at an intensity $\sim 10^{15}$ W/cm^2 onto a metal foil (25 μm thick Tungsten or aluminum foil, *interaction target*) in order to launch a shock wave in the surrounding atmosphere. CPA_2 was compressed down to a 300 fs duration and it was focused at an intensity in excess of 10^{18} W/cm^2 onto a thin metal foil (25 μm thick Tungsten, *proton target*) leading to the acceleration of a proton beam. The proton beam was used as transverse charged particle probe in a point projection scheme (*proton imaging*) for the electric fields generated at the irradiated side of the interaction target (see [6] for a typical experimental setup). In the low density regime for the probed plasma considered here, proton imaging is mainly sensitive to field gradients, which are detected via modulations in the proton density across the beam transverse section. The distance between the proton target and the interaction target was $l \sim 4$ mm and the distance between the interaction foil and the proton detector was $L \sim 3.6$ cm, giving a projection magnification $M = (l + L)/l \sim 10$. The proton beam was detected employing a stack of several layers of dosimetrically cali-

brated radiochromic films (RCFs). The multilayer arrangement of the detector together with the broad spectral content of the proton beam provided temporal multiframe capabilities for the proton probing line within a single laser shot.

Data exemplifying the typology of features observed in proton images are shown in Fig. 1(a). As a rule of thumb the electric fields are directed from the regions of a lighter blue color compared to the background (zones of reduced probe proton flux) towards the regions of darker blue color (increased flux). A region of pronounced modulation in the probe proton density, revealing a strongly modulated field distribution, is observed to extend from the irradiated target surface up to a distance ~200–300 μm from the laser focal spot (region I). Comparisons with optical interferometry data taken in dedicated shots and 2D hydrodynamic (POLLUX) simulations indicate that such a field distribution is associated with the dense region ($n_e > 10^{18}$ cm^{-3}) of the blow-off plasma produced by direct laser ablation of the target (see also [7]). Away from the target, in the low density background plasma ($n_e \lesssim 10^{15}$ cm^{-3}), several different structures are observed (regions II and III) which we interpret as shock waves propagating ahead of the ablating plasma. Such structures exhibit a spherical symmetry and appear to be radially expanding from the laser focal spot. In the equatorial region they are interrupted by the plasma channel created by the laser beam propagation, which is likely to alter the background plasma conditions therefore affecting the shock formation and propagation in this region. At a distance ~500 μm from the target, a series of 4-5 very localized arc-shaped modulations can be distinguished [region II and detail 1(b)]. Each modulation has a thickness of $\lesssim 10$ μm, while their relative distance ranges from ~30 to ~70 μm increasing in the outgoing radial direction. Further away, at a distance of ~1 mm from the focal spot, a clear modulation is observed, which has on the whole a semiannular shape with an average radius of curvature $R \sim 750$ μm and a thickness $\delta R \sim 50$ μm [region III and detail 1(d)]. Both the localized arc-shaped and the larger annular-shaped modulations consist of an annulus of proton depletion delimited by two thin rings of proton accumulation. This pattern reveals an electric field distribution characterized by a first region where the field points in the inward radial direction followed by a region where the field points in the outward direction. In some shots the annular-shaped modulation consisted of a periodic succession of regions of proton accumulation and depletion, revealing an oscillatory field distribution [region III, detail 1(h)]. Typically such an oscillatory packet had a width of ~80–90 μm with a characteristic oscillation length of ~30–40 μm, and therefore 2-3 oscillation periods could be distinguished. All these structures were observed to expand at a velocity $V \sim 2$–4×10^5 ms^{-1}, with the larger amplitude modulations moving at a larger velocity. The shock velocity was measured within single laser shots, as the shock front position appeared to be different in different RCF layers corresponding to different probing times. Note also that if we take the ratio between the shock front width and the shock velocity as a characteristic time for the shock motion $\delta R/V > 10^2$ ps, its value well exceeds the time of flight of the probe protons through the shock front, $b/v_p \sim 10$ ps (where $b \simeq 2\sqrt{(R+\delta R/2)^2 - R^2} \sim 390$ μm is the average extension of the electric field distribution along the probe proton path and v_p is the probe proton velocity), implying that the

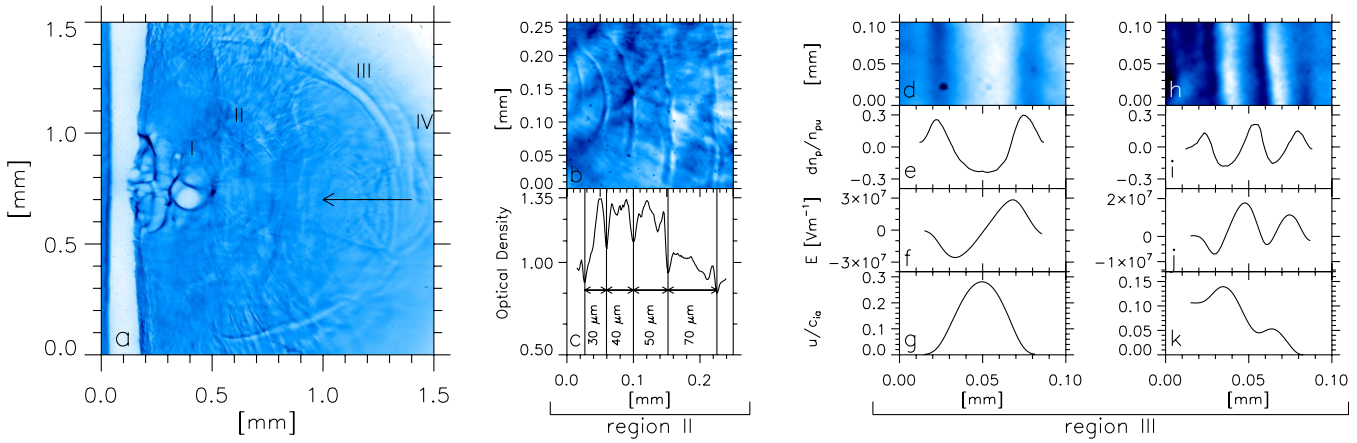

FIG. 1 (color online). (a) Typical proton imaging data taken at the peak of the interaction pulse with protons of 7 MeV energy. Note the strong modulation associated with the ablating plasma in the region I and the modulated pattern ahead of the shock front possibly associated with a reflected ion bunch in the region IV. The arrow indicates the laser beam direction. (b)–(c) Detail and RCF optical density lineout corresponding to the region II showing modulations associated with a train of solitons. (d)–(k) Details of the region III and correspondent lineouts of the probe proton density $\delta n_p/n_{\mathrm{pu}}$, reconstructed electric field E, and reconstructed normalized ion velocity u/c_{ia} in the case of an ion acoustic soliton (d)–(g) and of a collisionless shock wave (h)–(k) (the collisionless shock detail corresponds to a different shot not shown here for brevity).

observation is not substantially affected by time integration. Finally ahead of the larger annular structure a modulated region is observed (region IV), which extends, depending on the proton probing time, up to a distance of 50–100 μm from the larger annular-shaped structure and which expands at a velocity $\sim$2 V. It was also observed that the proton density modulation associated with such a pattern was more pronounced when the modulation in the region III had an oscillatory character.

We notice first of all that the observed shock structures must have a collisionless character and are likely to be nonmagnetized. In order to support this statements we estimate the various particle mean free paths and the electron Debye length in the background plasma and compare them to the measured shock front widths. We assume that the background air gas is fully dissociated and ionized, which corresponds to the minimum values for the various mean free paths and therefore to the most collisional case. We take the ion charge state to be $Z \simeq 7.2$ and the ion mass (in units of proton mass) to be $\mu \simeq 14.4$, which correspond to the average between nitrogen and oxygen ion charge states and masses, respectively, weighted according to the air composition at standard conditions. Moreover it is reasonable to assume that the background plasma is homogeneous, as it is created via photoionization of the residual gas in the vacuum chamber, and therefore that our estimations will equally apply to the regions II, III, and IV. We also verified that, in the regions II, III, and IV, POLLUX simulations did not show any sizeable contamination of the background plasma by the inhomogeneous ablating plasma. Given the experimentally measured average air pressure $p \sim (1\text{–}5) \times 10^{-3}$ mbar in the target chamber, a maximum ion and electron density of respectively $n_i \sim (5\text{–}25) \times 10^{13}$ cm^{-3} and $n_e = Zn_i \sim (3.5\text{–}20) \times 10^{14}$ cm^{-3} can be inferred. An electron temperature $k_B T_e \sim m_i V^2/Z \sim (1\text{–}3.5)$ keV can also be estimated by assuming that the shocks travel approximatively at the ion-acoustic velocity $c_{\mathrm{ia}} \sim V \sim (2\text{–}4) \times 10^5$ ms^{-1}. Finally, we approximate the ion velocity with the shock velocity V. Given these estimations, the electron-electron, electron-ion, and ion-ion mean free paths turn out to be all several cm or more and, therefore, are much larger than the shock width which is in the range (25–90) μm, ruling out the possibility that the observed shocks have a collisional character. Under the same assumptions the electron Debye length can be estimated to be $\lambda_{\mathrm{De}} \sim (5\text{–}20)$ μm, which is comparable with the shock widths, as expected for the case of nonmagnetized collisionless shocks.

We interpret our data within the framework of the weakly nonlinear wave description based on the KdV-B equation $\partial_t u + u\partial_x u + \beta\partial_{xxx} u = \nu\partial_{xx} u$, where $u(x, t)$ is the ion velocity [1]. The $u\partial_x u$ term is associated with convective nonlinearity and is responsible for wave steepening. In absence of a compensating mechanism, such as wave dispersion or energy dissipation, it would eventually lead to wave breaking. The $\beta\partial_{xxx} u$ term, where $\beta = \lambda_{\mathrm{De}}^2 c_{\mathrm{ia}}/2$, is associated with wave dispersion, and corresponds to the $(1/2)k^3 c_{\mathrm{ia}} \lambda_{\mathrm{De}}^2$ term in the long wavelength limit of the dispersion relation for ion-acoustic waves. The $\nu\partial_{xx} u$ describes energy dissipation, which can be due to viscosity and thermal conductivity and/or can be associated with collisionless phenomena such as ion reflection at the shock front, electron trapping in the shock, microturbolence, or others [2]. The expression for the ν coefficient depends in detail upon the dissipation mechanism. We adopt a planar model in view of the fact that the observed shocks have already undergone a substantial expansion by the time they are observed, this resulting in a small ratio $\delta R/R \ll 1$ between their width and their overall radius. We also verified that, for our experimental conditions, applying a two component plasma model [8] in order to account for the air plasma composition did not make a sizeable difference.

The structure of the shocklike stationary solutions admitted by the KdV-B equation depends on the relative role of nonlinearity, dispersion, and dissipation. In the dissipationless limit $\nu \ll \sqrt{\beta u_m}$ one can neglect the $\nu\partial_{xx} u$ term, obtaining the KdV equation, for which localized perturbations will asymptotically disperse for $t \to \infty$ into a train of solitons [1]. Each soliton in the train is described by $u(X) = u_m \cosh^{-2}(X/l_S)$ (where $X = x - Vt$ is the spatial coordinate in the reference frame moving with the shock), which has the shape of a localized bump [see Fig. 2(a), purple line] of width $l_S = \sqrt{12\beta/u_m}$ and propagating at a velocity $V = c_{\mathrm{ia}} + u_m/3 \simeq c_{\mathrm{ia}}$. When both dissipation and dispersion are taken into account an initial perturbation evolves into a collisionless shock wave, which in general has the form of a modulated jump with a stationary oscillatory character at the front [Fig. 2(b), blue line]. The electric field induced in the plasma is proportional to the ion acceleration in the laboratory reference frame $E = m_i(\partial_t u + u\partial_x u)/(Ze) \simeq -(m_i V)/(Ze)\partial_X u$. In the case of the soliton the electric field reads $E(X) \approx -(2m_i V u_m)/(Zel_S)\tanh(X/l_S)\cosh^{-2}(X/l_S)$, which has the form of a single period oscillation [Fig. 2(a), red line], while in the case of the collisionless shock wave it has an oscillatory character [Fig. 2(b), red line].

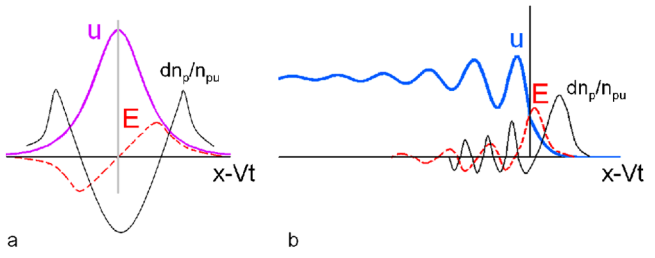

FIG. 2 (color online). Theoretical ion velocity u (purple and blue lines), electric field E (red lines) and expected probe proton density modulation $\delta n_p/n_{\mathrm{pu}}$ (black lines) for (a) an ion-acoustic soliton and (b) a collisionless shock wave.

In order to interpret our data we notice that in the limit of small deflections the proton density modulation can be related to the deflecting transverse (with respect to the probe proton propagation direction z) electric field $\mathbf{E}_\perp$ by the relation $\delta n_p/n_{\rm pu} \simeq -(eL)/(2\mathcal{E}_p M)\nabla_{\perp 0}\cdot\int_b \mathbf{E}_\perp dz$. Here, $\delta n_p = n_p - n_{\rm pu}$, with n_p and $n_{\rm pu}$ being, respectively, the perturbed and unperturbed proton densities measured at the detector plane, $\mathcal{E}_p$ is the probe proton energy and $\nabla_{\perp 0}\cdot$ is the divergence calculated with respect to the proton transverse coordinates at the interaction target plane. The expected proton density modulation in the case of the ion-acoustic soliton reads $\delta n_p/n_{\rm pu} \simeq (m_i V u_m L b)/(Z l_S^2 \mathcal{E}_p M)[\cosh(2X/l_S) - 2]\cosh^{-4}(X/l_S)$, while in the case of the collisionless shock wave it has an oscillatory character, as shown as black lines in Figs. 2(a) and 2(b). Comparison with Fig. 1 reveals that the proton density modulation $\delta n_p/n_{\rm pu}$ profiles observed in proton imaging data clearly resemble the patterns that are expected to be generated by a soliton train 1(c), an ion-acoustic soliton 1(e) and a collisionless shock-wave 1(i). In the same framework the modulation observed ahead of the larger amplitude shocks [Fig. 1(a), region IV] can be associated with some degree of wave breaking or with a precursor of streaming ions accelerated via reflection at the shocks front. The fact that the front of this modulation travels at a velocity which is approximately the double of the shock velocity is consistent with the latter interpretation. It should also be noticed that the modulation possibly associated with the reflected ions is more evident when a collisionless shock-wave rather than a soliton is observed, providing an indication that ion reflection could be the dissipation mechanism responsible for the transition from a soliton structure to a collisionless shock wave.

In order to obtain a better comparison between the experimental findings and the theory, the electric field profile at the shock front in the different cases was reconstructed via numerical integration of the observed proton density modulation, i.e., $E \simeq -(2\mathcal{E}_p M)/(eLb)\times\int \delta n_p/n_{\rm pu} dX$. The ion velocity distribution, i.e., the shock profile, was then obtained via numerical integration of the ion momentum equation $u/c_{\rm ia} \simeq -(Ze/m_i V)\int E dX$. It is important to stress that in reconstructing the electric field and ion velocity profiles no assumption was made on the fact that the observed structures are ion-acoustic solitons or collisionless shock waves. The reconstructed electric field E and normalized ion velocity $u/c_{\rm ia}$ profiles (or equivalently the normalized ion density modulation $\delta n_i/n_i \simeq u/c_{\rm ia}$, as implied by the continuity equation for $V \sim c_{\rm ia}$) are plotted in Figs. 1(f), 1(j) and 1(g), 1(k), respectively. Note the characteristic localized bell shape in the case of the soliton 1(g) profile and the characteristic modulated jump in the case of the shock wave 1(k) profile. Note also that taking, for example, the case of the ion-acoustic soliton, the shock amplitude $u/c_{\rm ia}$ as obtained from the reconstructed profile is about 25%–30% 1(g). This confirms the weak but finite nonlinear character of the observed structures, thus supporting the validity of the small amplitude approximation implicit in the KdV-B model. Moreover it can be verified that by choosing the electron temperature (as estimated from the soliton velocity) and density (as estimated from the experimentally measured gas pressure) within the experimental errors and considering different possible ionization degrees, it is possible to find a finite range of values for which the relations between amplitude, width and velocity typical of an ion-acoustic soliton are fulfilled. As an example considering the experimentally measured soliton width $l_S \sim \delta R/2 \sim 25\ \mu$m and assuming full ionization, if we take for the soliton velocity $V \sim 2\times 10^5\ \mathrm{ms}^{-1}$ and for the electron density $n_e \sim 10^{15}\ \mathrm{cm}^{-3}$, from the relation between soliton amplitude and width we obtain $u_m/c_{\rm ia} = 6\lambda_{\rm De}^2/l_S^2 \sim 30\%$, consistently with the reconstructed value above.

The authors acknowledge discussions with Y. Kourakis (QUB) and the support of the EU programme No. HPRI CT 1999-0052, of Grant No. E1127 from Region Ile-de-France, of EPSRC Grant No. EP/C003586/1 and funding by DFG TR 18 and GK 1203. S. V. B acknowledges support via the QUB-IRCEP scheme.

*l.romagnani@qub.ac.uk

[1] D. A. Tidman and N. A. Krall, *Shock Waves in Collisionless Plasmas* (Wiley-Interscience, New York, 1971); R. C. Davidson, *Methods in Nonlinear Plasma Theory* (Academic, London, 1972); R. K. Dodd *et al.*, *Solitons and Nonlinear Wave Equations* (Academic, London, 1982); F. F. Chen, *Introduction to Plasma Physics and Controlled Fusion* (Plenum, New York, 1984).
[2] R. Z. Sagdeev and C. F. Kennel, Sci. Am. **264**, 106 (1991).
[3] V. S. Berezinskii, S. V. Bulanov, V. A. Dogiel, V. L. Ginzburg, and V. S. Ptuskin, *Astrophysics of Cosmic Rays* (Elsevier, Amsterdam, 1990); K. Koyama *et al.*, Nature (London) **378**, 255 (1995).
[4] D. W. Koopman and D. A. Tidman, Phys. Rev. Lett. **18**, 533 (1967); A. R. Bell *et al.*, Phys. Rev. A **38**, 1363 (1988); N. C. Woolsey *et al.*, Phys. Plasmas **8**, 2439 (2001).
[5] S. O. Dean *et al.*, Phys. Rev. Lett. **27**, 487 (1971); J. E. Borovsky *et al.*, Astrophys. J. **280**, 802 (1984); T.-H. Tan and J. E. Borovsky, J. Plasma Phys. **35**, 239 (1986).
[6] M. Borghesi *et al.*, Phys. Rev. Lett. **88**, 135002 (2002); L. Romagnani *et al.*, Phys. Rev. Lett. **95**, 195001 (2005).
[7] A. J. Mackinnon *et al.*, Rev. Sci. Instrum. **75**, 3531 (2004).
[8] M. Q. Tran and P. J. Hirt, Plasma Phys. **16**, 617 (1974).